



U.S. Department of
Transportation

**Federal Railroad
Administration**

Variable Amplitude Fatigue Crack Growth Characteristics of Railroad Tank Car Steel Volume III

Office of Research
and Development
Washington, DC 20590

Notice

This document is disseminated under the sponsorship of the Department of Transportation in the interest of information exchange. The United States Government assumes no liability for its contents or use thereof.

Notice

The United States Government does not endorse products or manufacturers. Trade or manufacturers' names appear herein solely because they are considered essential to the objective of this report.

REPORT DOCUMENTATION PAGE*Form Approved
OMB No. 0704-0188*

Public reporting burden for this collection of information is estimated to average 1 hour per response, including the time for reviewing instructions, searching existing data sources, gathering and maintaining the data needed, and completing and reviewing the collection of information. Send comments regarding this burden estimate or any other aspect of this collection of information, including suggestions for reducing this burden, to Washington Headquarters Services, Directorate for Information Operations and Reports, 1215 Jefferson Davis Highway, Suite 1204, Arlington, VA 22202-4302, and to the Office of Management and Budget, Paperwork Reduction Project (0704-0188), Washington, DC 20503.

1. AGENCY USE ONLY (Leave blank)		2. REPORT DATE December 2006	3. REPORT TYPE AND DATES COVERED Final Report December 2006	
4. TITLE AND SUBTITLE Variable Amplitude Fatigue Crack Growth Characteristics of Railroad Tank Car Steel Volume III			5. FUNDING NUMBERS DB034/RR28	
6. AUTHOR(S) James H. Feiger and Peter C. McKeighan				
7. PERFORMING ORGANIZATION NAME(S) AND ADDRESS(ES) U.S. Department of Transportation Research and Innovative Technology Administration John A. Volpe National Transportation Systems Center 55 Broadway Cambridge, MA 02142-1093			8. PERFORMING ORGANIZATION REPORT NUMBER DOT-VNTSC-FRA-05-03	
9. SPONSORING/MONITORING AGENCY NAME(S) AND ADDRESS(ES) U.S. Department of Transportation Federal Railroad Administration Office of Research and Development 1120 Vermont Avenue, NW Mail Stop 20 Washington, DC 20590			10. SPONSORING/MONITORING AGENCY REPORT NUMBER DOT/FRA/ORD-06/04.III	
11. SUPPLEMENTARY NOTES				
12a. DISTRIBUTION/AVAILABILITY STATEMENT This document is available to the public through the National Technical Information Service, Springfield, Virginia 22161.			12b. DISTRIBUTION CODE	
13. ABSTRACT (Maximum 200 words) The load history that railroad tank cars experience has a significant variable amplitude characteristic. Although previous efforts have been directed toward understanding baseline fatigue crack growth behavior of TC-128B steel as a function of material lot, orientation, and environment, little is known regarding how load interaction impacts crack growth behavior in a typical tank car steel. Load interaction occurs when the variable amplitude character of the loading results in crack growth that differs as a function of load history effects in the wake of the crack. The focus of this testing effort was to determine empirically how TC-128B behaves under these types of simplified loading conditions. The data provided in this report links the constant amplitude-loading regime to the more complex variable amplitude-loading regime that tank cars experience during in-service use. The data can also be used as modeling guidelines to better understand the role of variable amplitude loading on TC-128B.				
14. SUBJECT TERMS Load history, variable amplitude loading, fatigue crack growth, loading conditions, displacement, crack length, crack growth rate, load interaction, load perturbations			15. NUMBER OF PAGES 44	
			16. PRICE CODE	
17. SECURITY CLASSIFICATION OF REPORT Unclassified	18. SECURITY CLASSIFICATION OF THIS PAGE Unclassified	19. SECURITY CLASSIFICATION OF ABSTRACT Unclassified	20. LIMITATION OF ABSTRACT Unlimited	

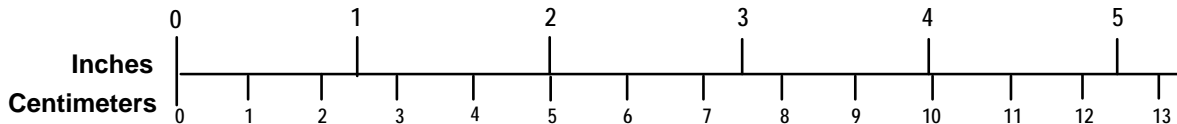
METRIC/ENGLISH CONVERSION FACTORS

ENGLISH TO METRIC

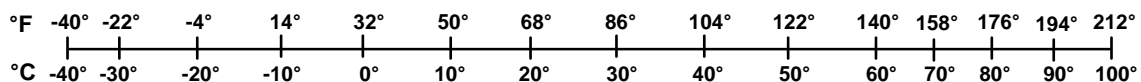
METRIC TO ENGLISH

<p>LENGTH (APPROXIMATE)</p> <p>1 inch (in) = 2.5 centimeters (cm)</p> <p>1 foot (ft) = 30 centimeters (cm)</p> <p>1 yard (yd) = 0.9 meter (m)</p> <p>1 mile (mi) = 1.6 kilometers (km)</p>	<p>LENGTH (APPROXIMATE)</p> <p>1 millimeter (mm) = 0.04 inch (in)</p> <p>1 centimeter (cm) = 0.4 inch (in)</p> <p>1 meter (m) = 3.3 feet (ft)</p> <p>1 meter (m) = 1.1 yards (yd)</p> <p>1 kilometer (km) = 0.6 mile (mi)</p>
<p>AREA (APPROXIMATE)</p> <p>1 square inch (sq in, in²) = 6.5 square centimeters (cm²)</p> <p>1 square foot (sq ft, ft²) = 0.09 square meter (m²)</p> <p>1 square yard (sq yd, yd²) = 0.8 square meter (m²)</p> <p>1 square mile (sq mi, mi²) = 2.6 square kilometers (km²)</p> <p>1 acre = 0.4 hectare (he) = 4,000 square meters (m²)</p>	<p>AREA (APPROXIMATE)</p> <p>1 square centimeter (cm²) = 0.16 square inch (sq in, in²)</p> <p>1 square meter (m²) = 1.2 square yards (sq yd, yd²)</p> <p>1 square kilometer (km²) = 0.4 square mile (sq mi, mi²)</p> <p>10,000 square meters (m²) = 1 hectare (ha) = 2.5 acres</p>
<p>MASS - WEIGHT (APPROXIMATE)</p> <p>1 ounce (oz) = 28 grams (gm)</p> <p>1 pound (lb) = 0.45 kilogram (kg)</p> <p>1 short ton = 2,000 pounds (lb) = 0.9 tonne (t)</p>	<p>MASS - WEIGHT (APPROXIMATE)</p> <p>1 gram (gm) = 0.036 ounce (oz)</p> <p>1 kilogram (kg) = 2.2 pounds (lb)</p> <p>1 tonne (t) = 1,000 kilograms (kg) = 1.1 short tons</p>
<p>VOLUME (APPROXIMATE)</p> <p>1 teaspoon (tsp) = 5 milliliters (ml)</p> <p>1 tablespoon (tbsp) = 15 milliliters (ml)</p> <p>1 fluid ounce (fl oz) = 30 milliliters (ml)</p> <p>1 cup (c) = 0.24 liter (l)</p> <p>1 pint (pt) = 0.47 liter (l)</p> <p>1 quart (qt) = 0.96 liter (l)</p> <p>1 gallon (gal) = 3.8 liters (l)</p> <p>1 cubic foot (cu ft, ft³) = 0.03 cubic meter (m³)</p> <p>1 cubic yard (cu yd, yd³) = 0.76 cubic meter (m³)</p>	<p>VOLUME (APPROXIMATE)</p> <p>1 milliliter (ml) = 0.03 fluid ounce (fl oz)</p> <p>1 liter (l) = 2.1 pints (pt)</p> <p>1 liter (l) = 1.06 quarts (qt)</p> <p>1 liter (l) = 0.26 gallon (gal)</p> <p>1 cubic meter (m³) = 36 cubic feet (cu ft, ft³)</p> <p>1 cubic meter (m³) = 1.3 cubic yards (cu yd, yd³)</p>
<p>TEMPERATURE (EXACT)</p> <p>$[(x-32)(5/9)]\text{ }^{\circ}\text{F} = y\text{ }^{\circ}\text{C}$</p>	<p>TEMPERATURE (EXACT)</p> <p>$[(9/5)y + 32]\text{ }^{\circ}\text{C} = x\text{ }^{\circ}\text{F}$</p>

QUICK INCH - CENTIMETER LENGTH CONVERSION



QUICK FAHRENHEIT - CELSIUS TEMPERATURE CONVERSION



For more exact and or other conversion factors, see NIST Miscellaneous Publication 286, Units of Weights and Measures. Price \$2.50 SD Catalog No. C13 10286

Updated 6/17/98

Table of Contents

1. Introduction.....	3
2. Material and Specimen Geometry	5
2.1 Phase A: Closure.....	5
2.2 Phase B: Over- and Under-Load Testing.....	5
3. Test Procedures.....	9
3.1 Phase A: Crack Closure Testing	9
3.2 Phase B: Over- and Under-Load Testing.....	10
3.2.1 Specimen B-2 (Specimen TCA16A)	10
3.2.2 Specimen B-1 (Specimen TCA18A)	10
4. Results and Discussion	13
4.1 Phase A: Closure.....	13
4.2 Phase B: Over- and Under-Load Testing.....	14
4.2.1 TCA16A (Test B-2: Over-Loads Only).....	14
4.2.2 TCA18A.....	15
5. Conclusions.....	29
Appendix A. Example of Crack Closure Analysis (Creation of the Reduced Displacement Data).....	31
Acronyms and Abbreviations	33

List of Tables

Table 1. Crack Ligament Required to Return to Steady-State Growth as Compared to Three Different Plastic Zone Size Estimations (TCA16A).....	17
Table 2. Number of Cycles Needed to Return to Steady-State Crack Growth (TCA16A)	17

List of Figures

Figure 1. M(T) Fatigue Crack Growth Specimen.....	6
Figure 2. Specimen Layout Schematic for C(T) Removal	6
Figure 3. Detailed C(T) Specimen Extraction Showing IDs	7
Figure 4. C(T) Fatigue Crack Growth Specimen.....	7
Figure 5. Over-Load Sequence for Specimen B-2.....	11
Figure 6. Over-Load/Under-Load Sequence for Specimen B-1	11
Figure 7. Fatigue Crack Growth Response for the Fully Reversed Condition	18
Figure 8. Load versus Displacement Plot (Three Cycles) for Specimen TCB6A ($2a/W = 0.45$, $K_{max} = 26 \text{ ksi}\sqrt{\text{in}}$).....	19
Figure 9. Reduced Displacement Plot for Specimen TCB6A ($2a/W = 0.45$, $K_{max} = 26 \text{ ksi}\sqrt{\text{in}}$).....	20
Figure 10. Crack Opening Load Ratio as a Function of Normalized Crack Length	20
Figure 11. Crack Closure Represented at ΔK_{eff}	21
Figure 12. Crack Length versus Cycle Count for Specimen TCA16A.....	22
Figure 13. Growth Rate as a Function of Normalized Crack Length	22
Figure 14. Number of Cycles Needed for Return to Steady-State Crack Growth.....	23
Figure 15. Stress Intensity Range as a Function of Normalized Crack Length.....	24
Figure 16. Fracture Surface Showing the Over-Load Events Applied During Testing of TCA16A	24
Figure 17. Crack Length versus Cycle Count for TCA18A (First Segment)	25
Figure 18. Crack Length versus Cycle Count for TCA18A (Second Segment).....	25
Figure 19. Crack Growth Rate as a Function of Normalized Crack Length (Events Shown).....	26
Figure 20. Crack Growth Rate versus Normalized Crack Length (First Segment).....	26
Figure 21. Crack Growth Rate versus Normalized Crack Length (Second Segment).....	27
Figure 22. Stress Intensity Range as a Function of Normalized Crack Length.....	27
Figure 23. Fracture Surface Showing the Over-Load Events Applied During Testing of TCA18A	28

Executive Summary

The load history that railroad tank cars experience has a significant variable amplitude characteristic. Load interaction occurs when the variable amplitude character of the loading results in crack growth that differs as a function of load history effects in the wake of the crack. Understanding how cracks respond to periodic over- and under-loads is an intermediate step linking baseline fatigue crack growth (FCG) rate data and behavior under full-spectrum loading conditions. The focus of this testing effort is to determine empirically how the basic material behaves under these types of simplified loading conditions.

The material investigated in this test effort was TC-128B, a commonly used steel in the fabrication of railroad tank cars. Testing was phased into two distinct efforts: crack closure at fully reversed loading (Phase A) and over- and under-load FCG interaction effects (Phase B). Servohydraulic test frames integrated with digital control systems were used to conduct modern FCG testing practices outlined in the American Society for Testing Materials (ASTM) E647 document. Techniques and test strategies based on decades of FCG testing at Southwest Research Institute (SwRI) were also used.

Crack closure levels of 40-50 percent were experienced for the $R = -1$ FCG testing. Both 2 and 5 percent closure levels were analyzed and demonstrated the same trend, with the 2 percent condition giving the higher closure level, which was expected. The overall FCG rate results were in excellent agreement with previous fully reversed testing performed in 2001.

For the over-load levels tested, transient crack growth behavior was observed at over-load greater than 50 percent. Crack growth retardation became very evident at 100-150 percent. In addition, at 200 percent over-load, crack growth was arrested with no signs of any crack extension after 20+ million cycles. The application of under-loads resulted in minimal transient effects in the crack growth rate behavior. The trends demonstrated in the over- and under-load study are in agreement with the accepted crack growth behavior as it relates to transient effects.

The data provided herein links the constant amplitude loading regime to the more complex variable amplitude loading regime which tank cars experience during in-service use. The data can also be used as modeling guidelines to better understand the role of variable amplitude loading on TC-128B.

1. Introduction

The load history that railroad tank cars experience has a significant variable amplitude characteristic. Although previous efforts (Part I) have been directed toward understanding baseline fatigue crack growth (FCG) behavior of TC-128B steel as a function of material lot, orientation, and environment, little is known regarding how load interaction impacts crack growth behavior in a typical tank car steel. Load interaction occurs when the variable amplitude character of the loading results in crack growth that differs as a function of load history effects in the wake of the crack.

The Federal Railroad Administration (FRA) has tasked the Volpe National Transportation Systems Center (Volpe Center) to better understand FCG behavior during and following over- and under-loads. Since periodic inspections for cracks are required for safe operation of tank cars that typically carry hazardous materials, accounting for variable amplitude loading history effects can be viewed as a critical element in developing an appropriate inspection strategy.

An intermediate step linking baseline FCG rate data and behavior under full-spectrum loading conditions is understanding how cracks respond to periodic over- and under-loads. The focus of this testing effort is to determine empirically how the basic material behaves under these types of simplified loading conditions. The testing presented herein was conducted in two phases. The first phase revisited Volpe Center Part I and closure as it relates to $R = -1$ loading conditions. The second phase of this effort focused on over- and under-loading conditions and the material response.

Only three of the described five tests were completed because of prioritization changes requested by the Volpe Center as testing progressed. These prioritization changes occurred as a consequence of (a) personnel changes at the Volpe Center and (b) recent draft National Transportation Safety Board (NTSB) reports from the Minot, North Dakota, tank car accident.

2. Material and Specimen Geometry

The material used in this program was tank car steel TC-128B, a steel commonly used in the fabrication of railroad tank cars. The first SwRI test project¹ provides a complete description of the material used in this program. When possible, test specimens remaining from the previous effort were used. The overall goal was to test the same material as in the previous program to eliminate material variability.

2.1 Phase A: Closure

SwRI used coupons remaining from Volpe Part I in this phase of testing. More specifically, middle-crack tension (M(T)) FCG specimens were used to perform the $R = -1$ FCG testing. A total of two M(T) specimens were slightly modified (grip configuration) and prepared for testing. The overall thickness, B , was 0.25 inch with an overall width of 4 inches. Figure 1 illustrates the M(T) configuration used in this effort. An electrical discharge machined (EDM) notch was machined into the specimen with an initial length, $2a$ of 0.8 inch. SwRI polished the region of anticipated crack growth to facilitate visual crack length determination.

2.2 Phase B: Over- and Under-Load Testing

The crack growth testing performed in this phase used the compact tension, (C(T)) specimen geometry. Figures 2 and 3 show that coupons were removed from the provided Material A. A total of 18 $W = 3$ -inch C(T) specimens (Figure 4) were fabricated for testing. The specimen thickness, B , was 0.225 inch, the same dimension as used during the first Volpe Center program. It is important to note that two specimens were removed through-thickness to maximize material usage. Specimens were EDM-notched to an initial length of $a/W = 0.2$. SwRI also polished these specimens to facilitate visual crack length measurements during testing.

¹ P.C. McKeighan and J.H. Feiger, "Fatigue Crack Growth Behavior of Tank Car Steel TC128B Subjected to Various Environments," Southwest Research Institute Project No. 18.03630, Final Report, September 2001.

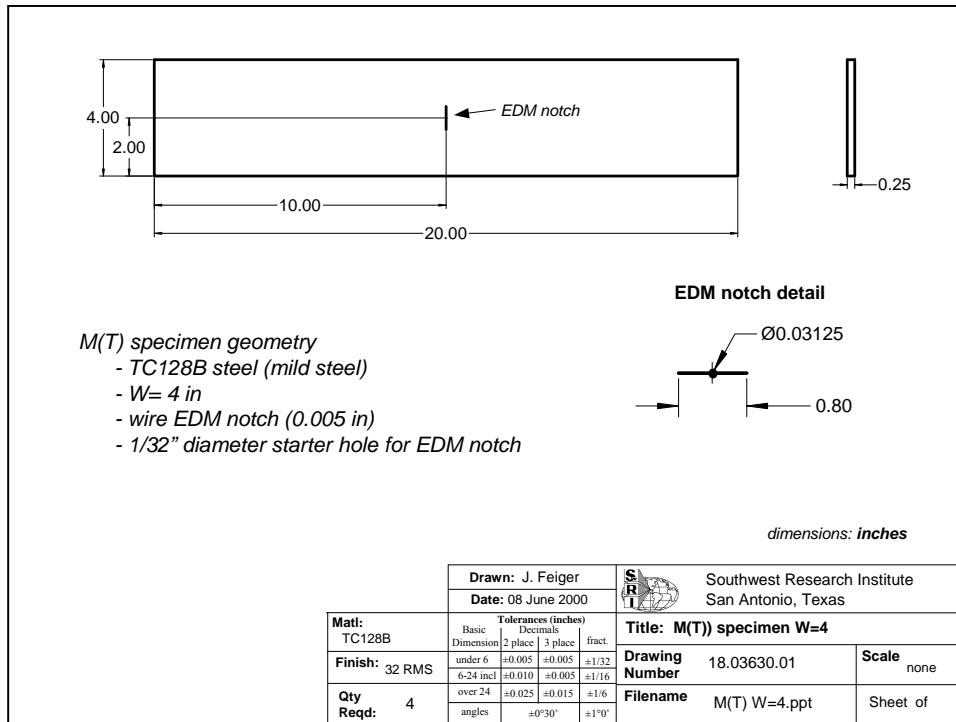


Figure 1. M(T) Fatigue Crack Growth Specimen

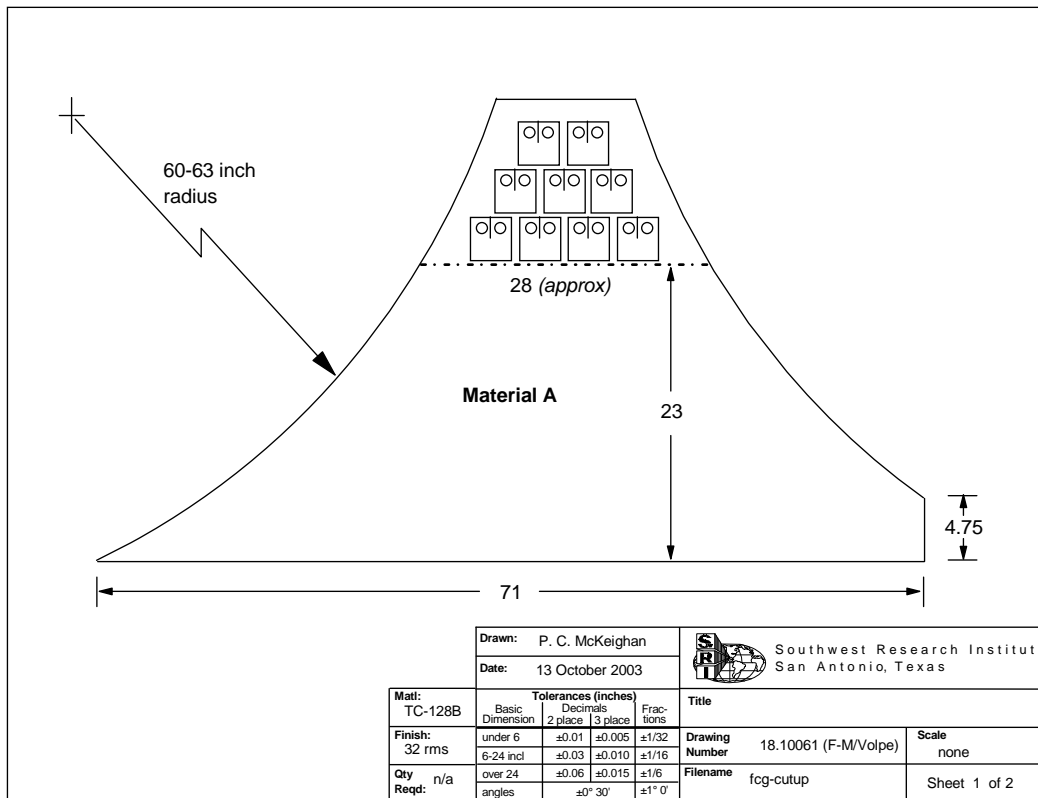


Figure 2. Specimen Layout Schematic for C(T) Removal

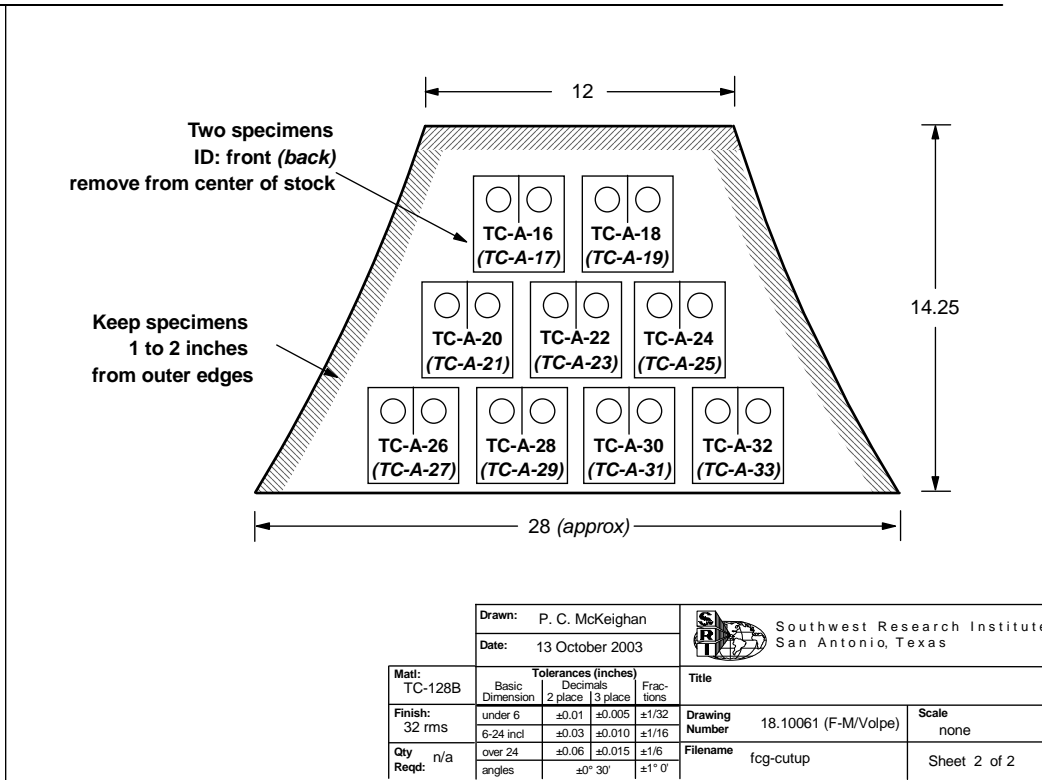


Figure 3. Detailed C(T) Specimen Extraction Showing IDs

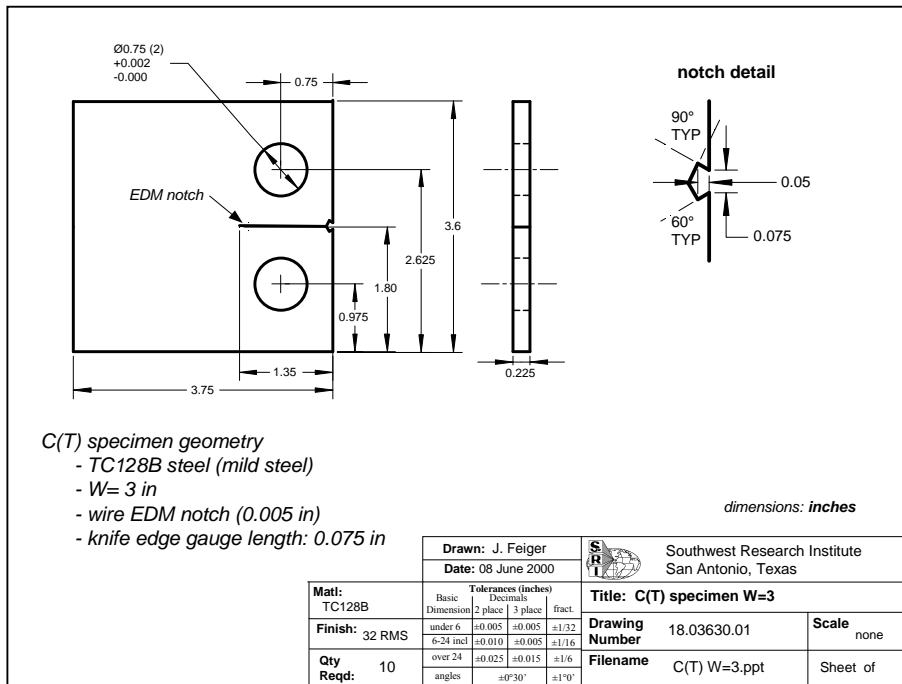


Figure 4. C(T) Fatigue Crack Growth Specimen

3. Test Procedures

3.1 Phase A: Crack Closure Testing

SwRI used a 50-kip servohydraulic test frame to conduct the FCG testing on the M(T) test coupons. Mechanical clamp grips were used to secure the specimen during loading. A Fatigue Technology Associates (FTA) digital control and supervision system was integrated with an MTS 458 analog controller to perform the fatigue testing. A fully reversed $R = -1$, stress ratio was used during this fatigue test. SwRI performed all testing in laboratory-air ambient conditions.

Crack length monitoring and closure measurements were made with two independent transducers. For the crack length determination, SwRI used a direct current potential drop (DCPD) that included an active probe pair and reference probe pair. The active and reference probe-to-probe placement was 0.25 inch and 6 inches, respectively. Closure data was generated with two 0.2-inch gage length clip gages secured on both sides of the specimens. Clip gages (extensometers) provide a highly accurate displacement measurement on the face of the FCG specimens. Knife edges were epoxy-bonded to the specimen surface to provide the relative measurement points and secure the clip gages. Epoxy was used to ensure electrical insulation from the DCPD system so as not to provide an alternate current path. Both clip gages were calibrated to the same range (0.01-inch full scale), and the two signals were processed with an averaging cable. In addition, the load and clip gage signal was filtered to achieve data suitable for closure analysis. SwRI used a LabVIEW data acquisition system to collect the closure data.

Specimen precracking was performed per the recommended ASTM E647 guidelines.² The EDM notch machined into the specimens was $2a = 0.8$ inch. Precracking involved loading the specimen at a constant ΔK of $6 \text{ ksi}\sqrt{\text{in}}$ at an R-ratio of -1. The final target precrack length ($2a$) was 0.9 in or $2a/W$ of 0.225 in. Upon completion of precracking, both crack-tips were measured, and the final maximum load was recorded.

FCG testing involved a K-increasing strategy, which included initially applying a ΔK of $6 \text{ ksi}\sqrt{\text{in}}$ with a K-gradient of 6 in^{-1} . Closure readings were initially scheduled for every $1 \text{ ksi}\sqrt{\text{in}}$, continuing until specimen failure. During closure readings, an independent ramping program, which included three cycles (1Hz) from zero-load to the current maximum load, was performed. Throughout the test, visual crack length measurements were made for post-test processing of the FCG data.

² ASTM E647-00, "Standard Test Method for Measurement of Fatigue Crack Growth Rates," *Annual Book of ASTM Standards 2004, Vol. 03.01*. ASTM International, West Conshohocken, PA.

3.2 Phase B: Over- and Under-Load Testing

A 10-kip servohydraulic test frame was used to conduct the over-load/under-load FCG testing on the C(T) test specimens. SwRI used clevis grips, as required by ASTM E647, to load the specimen. An FTA digital control system integrated into an MTS analog controller was utilized to conduct the testing. Two test sequences, which included varying levels of over-loads and under-loads, were executed and will be described. Only two of the required four tests were performed at the request of the Volpe Center. Crack length monitoring was performed with a clip gage mounted on the front face of the specimen. In addition, visual crack lengths (front and rear surfaces) were recorded for post-test processing of the data. All testing was performed in laboratory-air ambient conditions. The automated FTA test control system automatically performed crack closure monitoring.

Before conducting the over-load/under-load testing, the specimens were precracked per the recommended ASTM E647 practices. The final target length after precracking was an a/W of 0.25. Precracking was performed at loads substantially lower than the primary loading to minimize load-history effects. The main objective of this phase of testing was to characterize the retardation/acceleration effects due to over-loads and under-loads. The following sections describe these load perturbations.

3.2.1 Specimen B-2 (Specimen TCA16A)

Figure 5 presents the over-load sequence for specimen B-2. A constant ΔK strategy was employed, with over-loads induced periodically. The constant ΔK range used for this test was 10 $\text{ksi}\sqrt{\text{in}}$ at an R-ratio of 0.05. Over-loads were initiated at 25 percent (based on K_{max}) and increased in the following order: 25, 50, 75, 100, 150, and 200 percent. The appropriate time to apply the over-load was based on various criteria, with the two main variables being crack growth increment from the previous over-load (plastic zone size) and FCG rate (return to steady-state).

3.2.2 Specimen B-1 (Specimen TCA18A)

Although similar to specimen B-2 with respect to overall approach, specimen B-1 had over-loads and under-loads included in the scheduled sequence of events (Figure 6). In addition, the constant ΔK range and R-ratio were different for this specimen. A ΔK range of 5 $\text{ksi}\sqrt{\text{in}}$ and an R-ratio of 0.833 were used for the steady-state growth. The over-load and under-load levels were based on K_{max} . Similar to the test sequence used for specimen B-2, the application of the load perturbations was based on the crack growth increment from the previous event and achieving steady-state FCG. As testing progressed, the severity of the over-load/under-load increased, as is shown in Figure 6. In addition to the sequence outlined for specimen B-1, additional under-loads were applied in the following order: 22.5, 40, 50, 100, and 0 percent. This sequence was performed based on the results of the first segment.

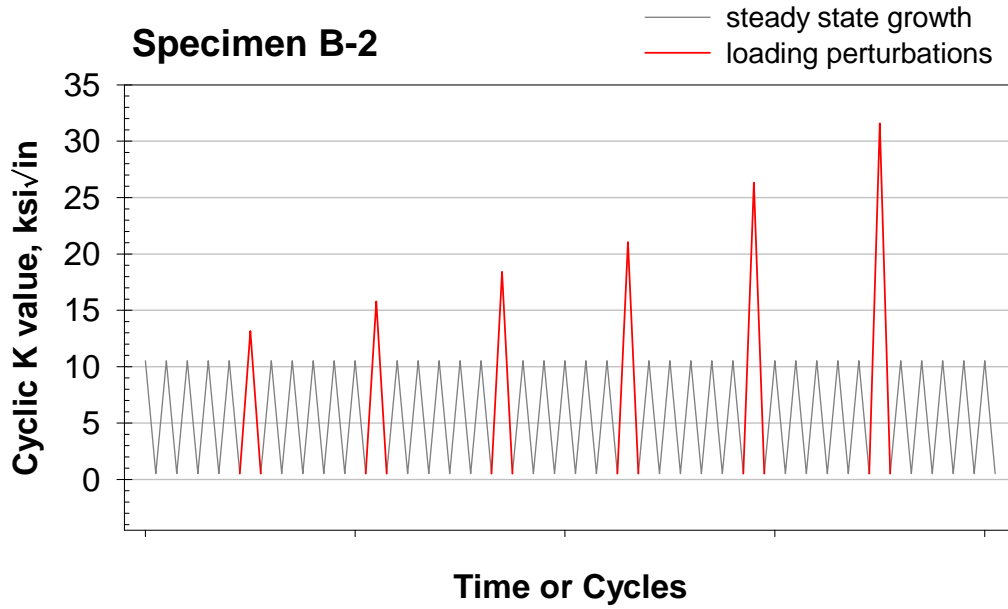


Figure 5. Over-Load Sequence for Specimen B-2

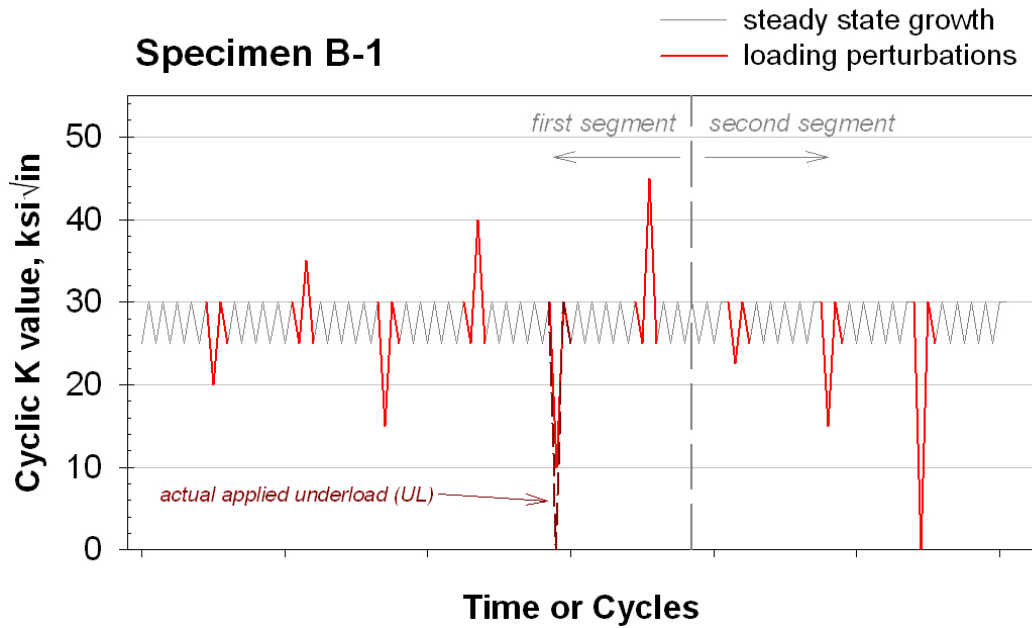


Figure 6. Over-Load/Under-Load Sequence for Specimen B-1

4. Results and Discussion

4.1 Phase A: Closure

Figure 7 presents the FCG results for the fully reversed FCG test (TCB6A). Figure 7 also shows the fully reversed crack growth results for the first Volpe Center test program. For the fully reversed test case and the results provided, ΔK is based on stress intensity range from the maximum stress intensity to zero load, or $\Delta K = K_{\max}$.

The agreement between the two tests is excellent, with a slight deviation in behavior at the higher growth rates. The difference noted, however, is well within the expected scatter typically observed during FCG rate testing. As testing progressed, the crack-tip asymmetry progressively increased, a common problem with the M(T) geometry. At no time, however, did the asymmetry violate that allowed by E647. This was also the case for the M(T) specimen tested during the first Volpe Center test program. This asymmetry is typically a consequence of residual stress in the specimen.

An important objective during the FCG testing of the M(T) specimen was collecting closure data for subsequent analysis. Data from the load/unload ramps were analyzed to determine the closure levels throughout the test. An automated software program was used, which allowed quick processing of the closure data. The program allows the user to investigate the variables associated with closure analysis and the effects of each. Overall, the results of the analysis are summarized in an output file allowing the user to critique the closure data. Appendix A shows an example of an output file.

The baseline data used to evaluate crack closure is applied load versus crack mouth opening displacement. Analysis of incremental slopes of the load-displacement response is used to determine the reduced displacement offset relationship and ultimately the crack closure level. Figure 8 shows representative load-displacement plots for specimen TCA-6A. In addition, the reduced displacement plot is provided (Figure 9), which illustrates the departure from linearity of the load-displacement behavior (crack closure). The knee demonstrated in the load versus displacement plot(s) is represented in the reduced displacement plot by a deviation from the zero offset line. The x-axis represents the percent deviation from the baseline slope. Closure levels, or opening load, are based on the amount of deviation, typically between 1 and 5 percent, represented on the reduced offset displacement plot. For this test, the 2 and 5 percent offset closure level was determined for the load and unload portion of a cycle. Figure 10 provides the closure levels, U , as a function of normalized crack length for the 2 and 5 percent offset criteria.

Figure 11 presents the implication of the crack closure on da/dN versus ΔK properties, which illustrates a shift to the left in the FCG data as a result of crack closure. Included in the FCG rate plot are the 2 and 5 percent offset closure levels; as expected, the 2 percent offset results in higher levels of reported crack closure.

4.2 Phase B: Over- and Under-Load Testing

The key aspect of Phase B was to investigate the FCG transient behavior after an over- or under-load event. More specifically, the crack growth behavior was monitored before and after a load perturbation. Fatigue crack growth data was recorded continuously throughout the test and used to characterize the transient behavior. In a classical sense, over- and under-load events are characterized by crack growth retardation or acceleration. A return to steady-state FCG occurs when the growth rate returns to the same rate as before the event and the crack grows out of the wake associated with the load perturbation.

4.2.1 TCA16A (Test B-2: Over-Loads Only)

The test was performed in a constant ΔK control mode; as such, the growth rate, outside the effects of the over- and under-load events, should remain constant. Under ideal conditions, a constant ΔK test will result in a constant growth rate. On a crack length versus cyclic life plot, a constant ΔK test results in a linear response with a constant slope (growth rate).

For specimen TCA16A, Figure 12 shows the crack length versus cycle. Indicated on this plot are the over- and under-load events to demonstrate the effects of the perturbations. An increase in the slope indicates an increase in the growth rate. Similarly, a decrease in the slope indicates a decrease in the growth rate. When analyzing the crack length versus cycle count data, deviations from the steady-state growth rate begin to occur at the 75 percent over-load level. Furthermore, as the severity of the over-load increases (higher over-load level), the slope decreases indicating more crack growth retardation. At the 150 percent over-load level, the level of crack growth retardation is severe, with a long cyclic duration before, returning to steady-state. For the 200 percent over-load condition, the crack was arrested with no measurable crack growth after 20+ million applied cycles. The test was terminated at that point.

The level of crack growth retardation can also be presented on a crack growth rate versus crack length plot, as shown in Figure 13. From the data presented, as the level of over-load increases the amount of specimen ligament required to return to steady-state also increases. This behavior presumably results from the over-load plastic zone size and the residual stresses that are developed in the wake of the crack over-load. Figure 12 shows the sensitivity inherent in a crack growth rate measurement for detecting over-load effects. As seen in the figure, noticeable deviations in the a versus N behavior occur at an over-load level of 75 percent. A close examination of Figure 13, however, clearly shows a slight perturbation in growth rate apparent at the lower 50 percent over-load level.

Table 1 presents the crack growth interval required after an event in order to return to steady-state FCG. Table 1 also presented the plastic zone sizes, based on the over-load level, for the plane stress, plane strain, and Irwin plastic zone sizes. When comparing the estimated plastic zone sizes to the crack ligament needed to return to steady-state, the amount of crack growth needed is between the plane stress and the Irwin plastic zone size estimations. A yield stress of 58 ksi was used in the plastic zone size estimations. Along with the crack length needed to return to steady-state, it is important to report the number of cycles after each event that are required to return to steady-state. Table 2 and Figure 4 show these data. As would be expected,

the more severe the over-load event, the greater number of cycles required to return to steady-state growth (ΔN). The difference between a 50 and 150 percent over-load is on the order of 10x.

Closure data was also collected throughout the test for specimen TCA16A. Figure 15 presents the stress intensity range, both applied and effective. The applied constant ΔK for the duration of the test was 10-ksi $\sqrt{\text{in}}$. The effective ΔK range initially started out at 7.5 ksi $\sqrt{\text{in}}$ and gradually increased to 8 ksi $\sqrt{\text{in}}$ before the 100 percent over-load event. After the 100 percent over-load, the effective stress intensity slightly decreased to approximately 7.75 ksi $\sqrt{\text{in}}$. After the 150 percent over-load, the effective stress intensity increased to slightly over 8 ksi $\sqrt{\text{in}}$ and gradually decreased to near 7 ksi $\sqrt{\text{in}}$. It is unclear what happened regarding the 150 percent over-load and the effective stress intensity range. One possibility could be related to the residual stresses associated with the over-load and their role in closure. The trend of a decrease in closure (i.e., higher effective ΔK levels) is somewhat counterintuitive given that the specimen was subjected to tensile over-loads. One would normally expect a decrease in closure to lead to faster growth rates, not slower rates indicative of an over-load zone.

Macroscopic photographs of the failed TCA16A specimen fracture surface were taken. Figure 16 shows the fracture surface. The appearance is typical of steels and is characterized as flat and with few noticeable features other than the over-load events. Over-loads were readily observable at and above the 100 percent over-load level.

4.2.2 TCA18A

In addition to over-loads, under-loads were included in the loading history for test specimen TCA18A. A constant ΔK of 5 ksi $\sqrt{\text{in}}$ and an R-ratio of 0.83 were used for the steady-state FCG segments. This loading condition results in a relatively slow FCG rate on the order of $2(10^{-8})$ in/cycle. Similar to the test specimen TCA16A, the application of an event (over- or under-load) was based on the steady-state FCG rate. The magnitude of the over-load is based on the maximum stress intensity for the steady-state loading.

Figures 17 and 18 provide the crack length versus cycle count for specimen TCA18A. Two segments are presented. The first segment includes the schedule outlined for specimen B-1. In addition, three more under-load events were performed to further investigate the crack growth behavior and are presented in the second segment. Before performing the second segment of testing, the crack-tip was reconditioned at the steady-state loading conditions. When interpreting the crack length versus cycle count data for both segments, very little influence occurs on the FCG rate for the over- and under-load events. Slight deviations from the steady-state growth rate exist, but the transient behavior is short-lived. This is expected, as the over- and under-load events were less severe than those performed on specimen TCA16A.

Figures 19 through 21 present the growth rate versus normalized crack. Figure 19 provides the overall response, while Figures 20 and 21 present the first and second segments. One note of interest regarding the two segments is the noticeable difference between the steady-state growth rates. For the first segment the FCG rate is nominally $2(10^{-8})$ in/cycle, while for the second segment the steady-state growth rate is near $7(10^{-8})$ in/cycle. This difference is likely a

consequence of the arrest and reconditioning after over-load #6. When the crack was arrested, growth was restarted by decreasing K_{\min} (K_{\max} remained fixed). The slight elevation in growth rate was likely a consequence of the load history effects during the crack tip reconditioning.

For the under-load events performed, the only condition that appears to affect the crack growth rate is the 100 percent under-load or a complete unload of the specimen. Based on the two 100 percent under-loads, the crack growth rate is retarded slightly and then eventually returns to steady-state conditions. The over-load levels tested were relatively low, and as such the crack growth retardation was also low. The 150 percent over-load, at the end of the first segment, resulted in crack growth arrest, and the test was eventually terminated after 10+ million cycles. The 133 percent over-load resulted in a slight perturbation in the growth rate, but a rapid return to steady-state conditions was experienced.

The stress intensity, both applied and effective, was evaluated as a function of crack length for specimen TCA18A and is presented in Figure 22 for the first and second segments. The consistency of the applied ΔK was excellent for the entire test. In addition, the effective stress intensity remained constant at approximately $3.4 \text{ ksi}\sqrt{\text{in}}$ as compared to the applied stress intensity of $5 \text{ ksi}\sqrt{\text{in}}$. The over- and under-load events do not appear to influence the closure behavior at these loading conditions.

Fractographs were taken of specimen TCA18A, as well of a representative image shown in Figure 23. The first and second segments of events are indicated on the image. The appearance of corrosion on the first segment occurred during the testing of the second segment and is presumably a result of the long duration of testing and exposure to ambient humidity. Overall, and similar to specimen TCA16A, the appearance is flat, with few surface features. The events of both segments are discernible upon close examination. The crack front was very symmetrical throughout the test, as is shown in the image.

Table 1. Crack Ligament Required to Return to Steady-State Growth as Compared to Three Different Plastic Zone Size Estimations (TCA16A)

Over-Load (%)	K _{OL} (ksi √in)	Δa (in)	Plastic Zone Size		
			Plane Strain r _y (in)	Plane Stress r _y (in)	Irwin r _y (in)
50	15.8	0.016	0.004	0.012	0.024
75	18.4	0.018	0.005	0.016	0.032
100	21.1	0.033	0.007	0.021	0.042
150	26.3	0.057	0.011	0.033	0.066

*No Detectable Retardation Occurred After the 25 Percent Over-Load

Equations: plane strain $r_y = \frac{1}{6\pi} \left(\frac{K}{\sigma_y} \right)^2$

plane stress $r_y = \frac{1}{2\pi} \left(\frac{K}{\sigma_y} \right)^2$

Irwin $r_y = \frac{1}{\pi} \left(\frac{K}{\sigma_y} \right)^2$

Table 2. Number of Cycles Needed to Return to Steady-State Crack Growth (TCA16A)

Over-Load (%)	Cycle Count Over-Load Event	Cycle Count Steady State	ΔN
50	423,497	496,000	72,503
75	629,269	712,000	82,731
100	855,019	1,063,200	208,181
150	1,204,528	2,022,500	817,972
200	2,216,670	crack arrest (20+ million)	

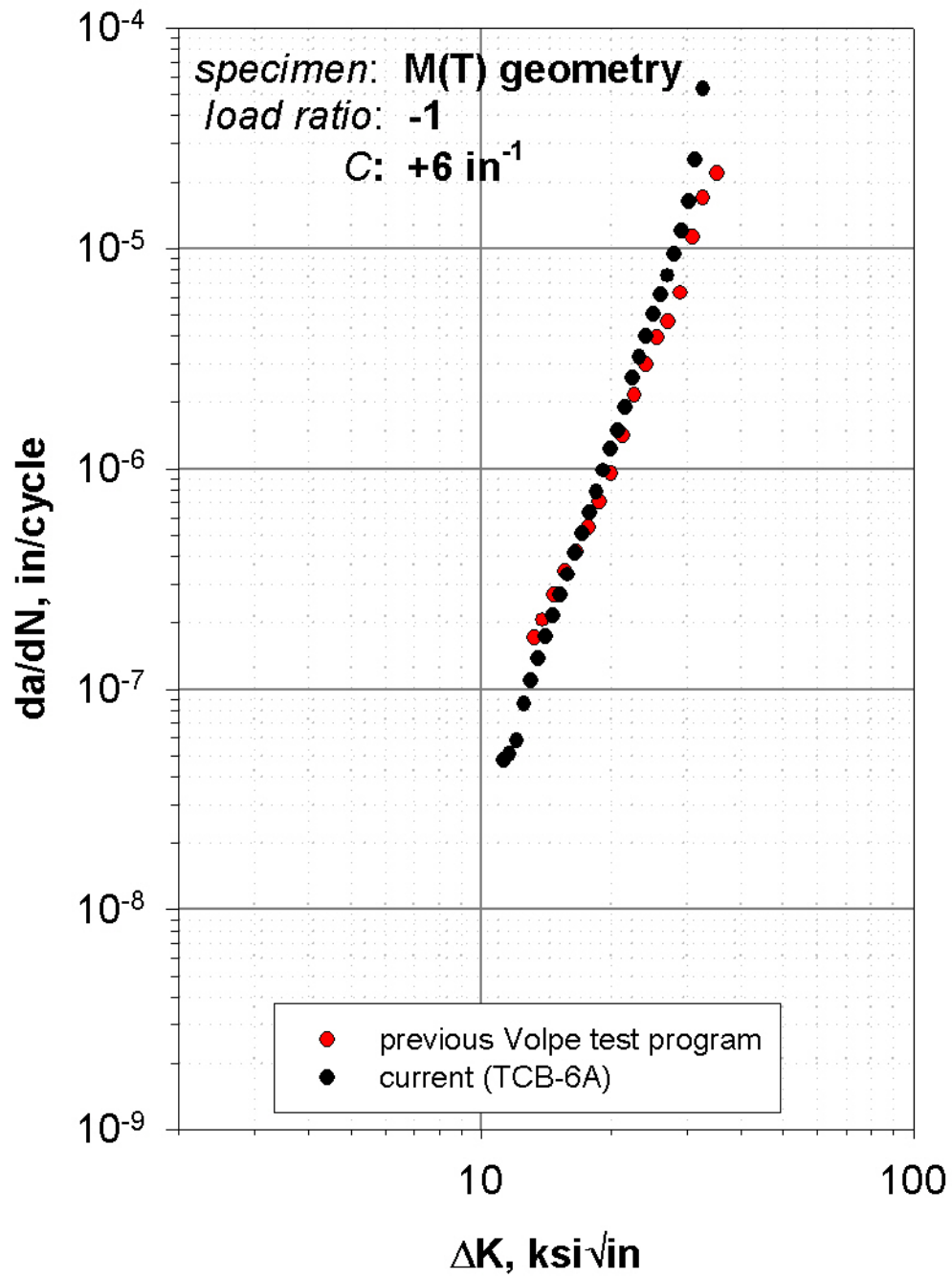


Figure 7. Fatigue Crack Growth Response for the Fully Reversed Condition

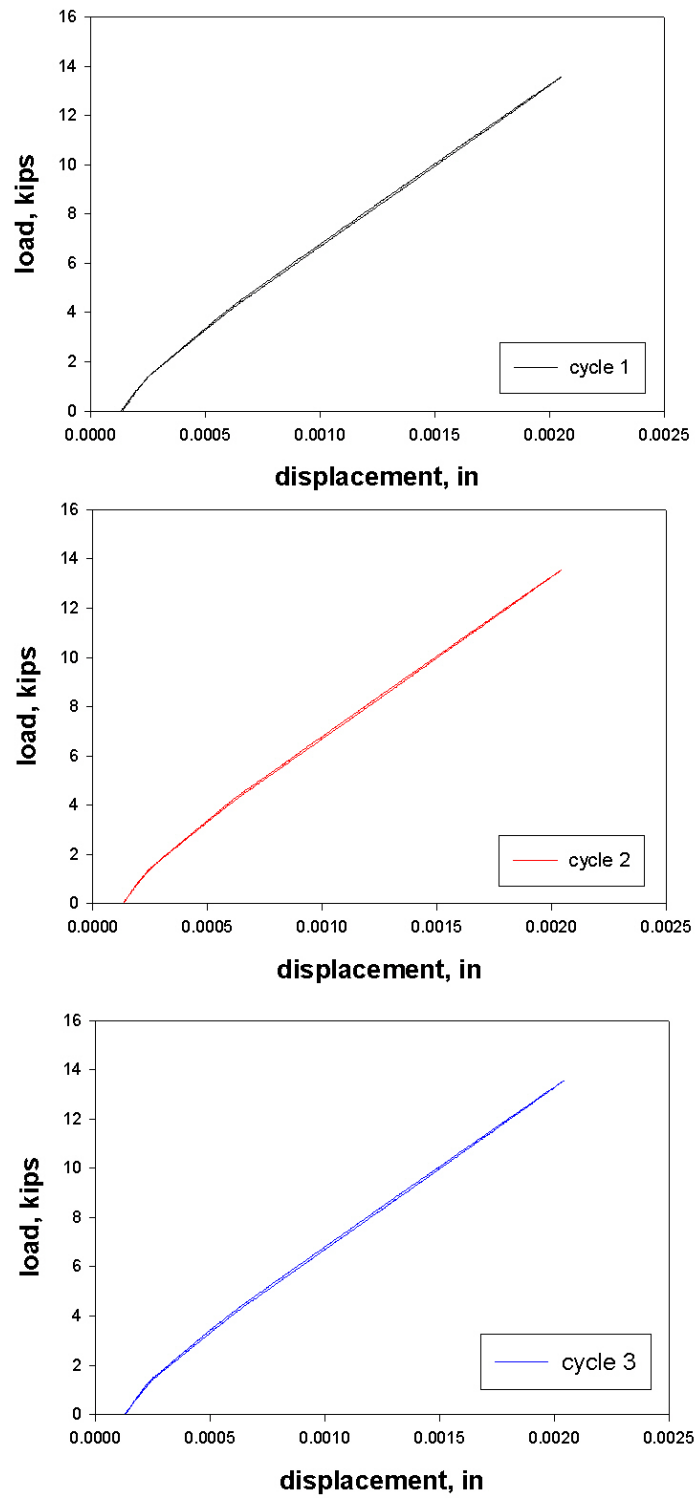


Figure 8. Load versus Displacement Plot (Three Cycles) for Specimen TCB6A ($2a/W = 0.45$, $K_{max} = 26 \text{ ksi}\sqrt{\text{in}}$)

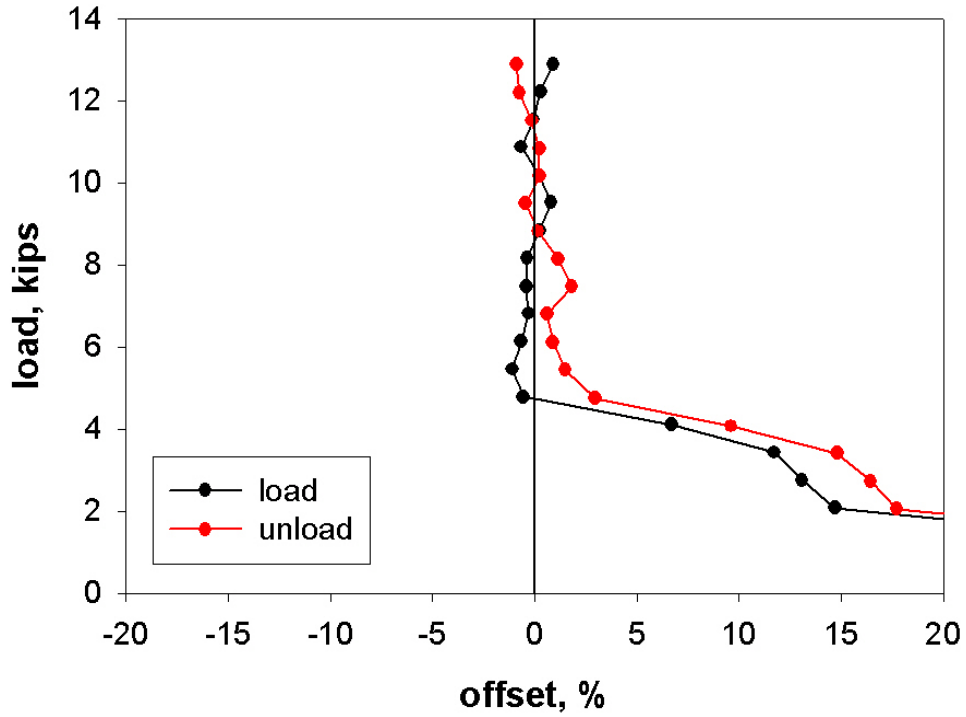


Figure 9. Reduced Displacement Plot for Specimen TCB6A ($2a/W = 0.45$, $K_{max} = 26 \text{ ksi}\sqrt{\text{in}}$)

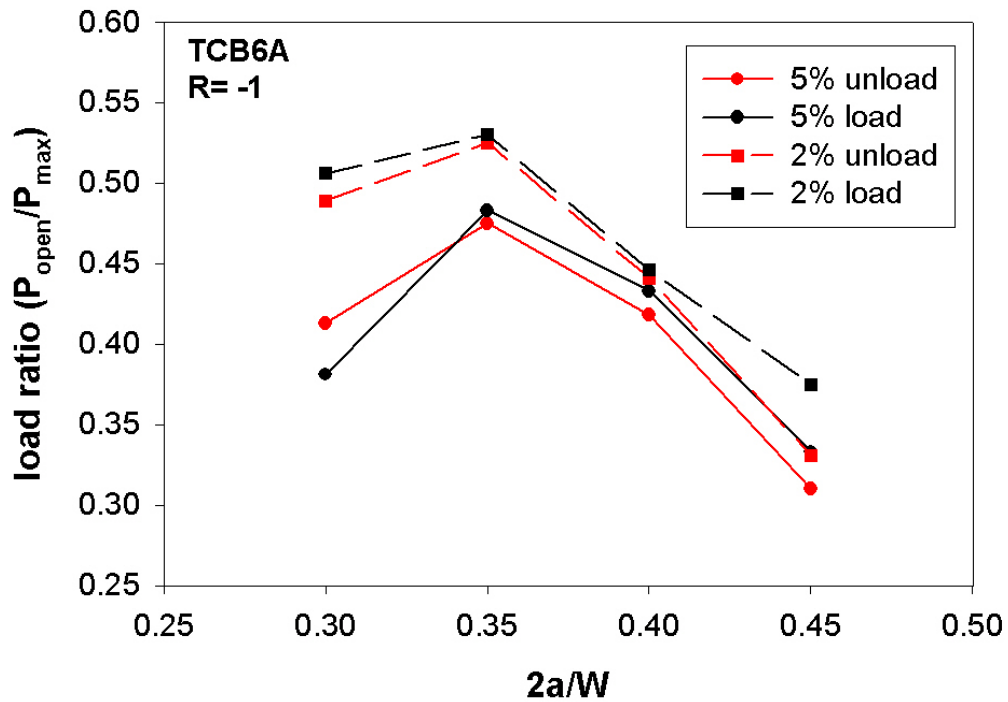


Figure 10. Crack Opening Load Ratio as a Function of Normalized Crack Length

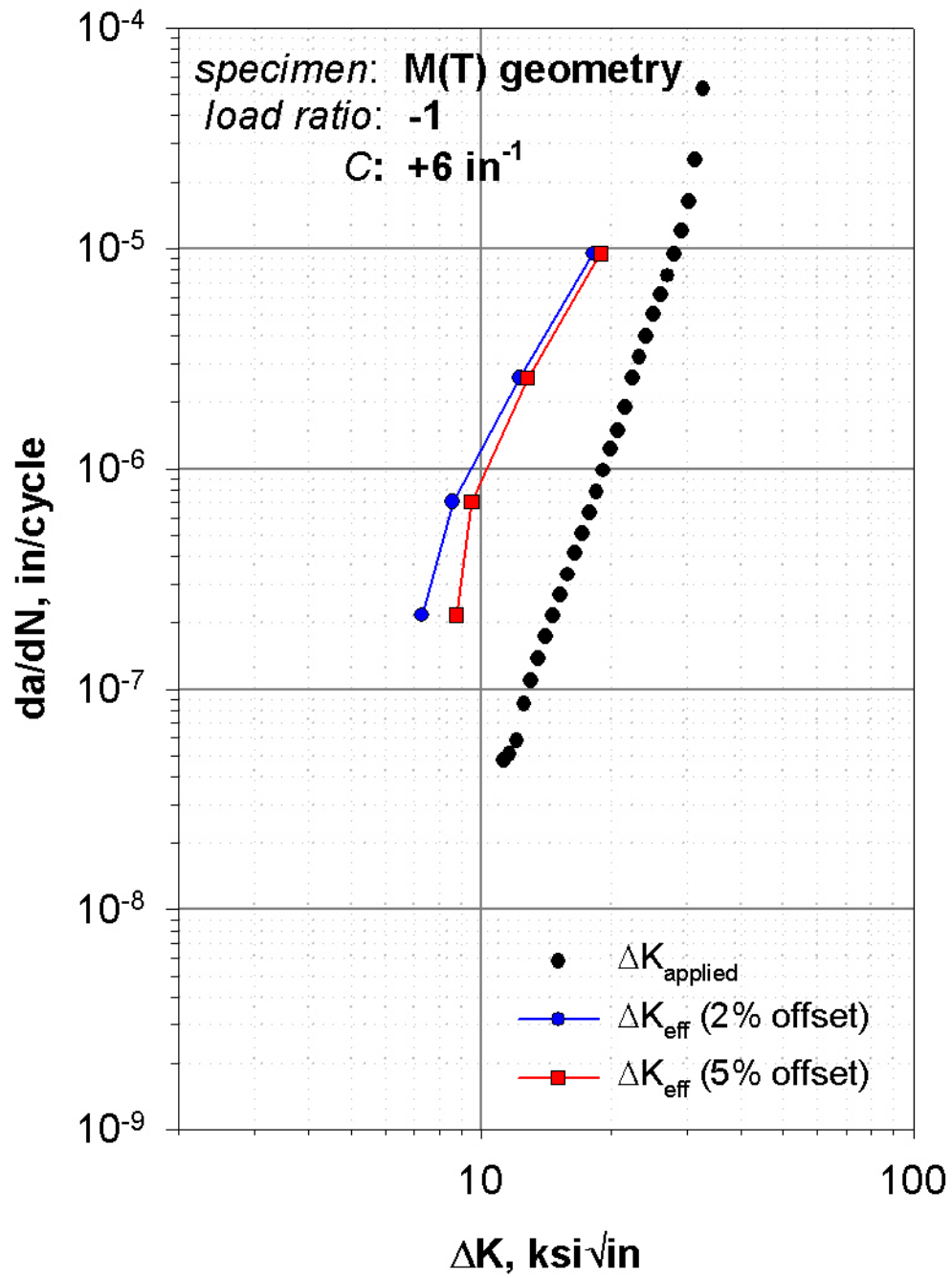


Figure 11. Crack Closure Represented at ΔK_{eff}

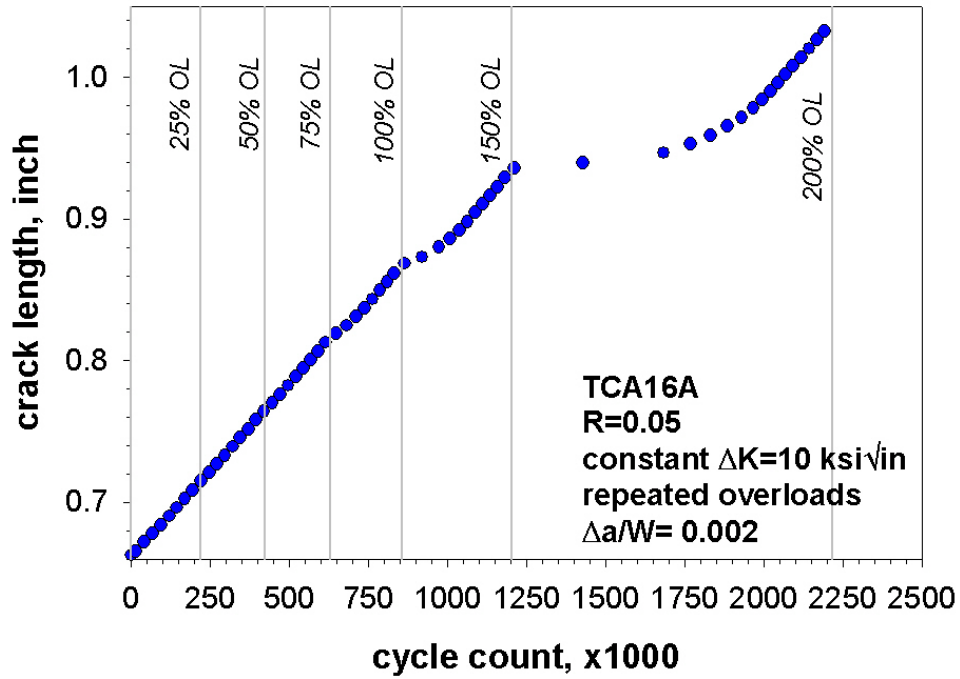


Figure 12. Crack Length versus Cycle Count for Specimen TCA16A

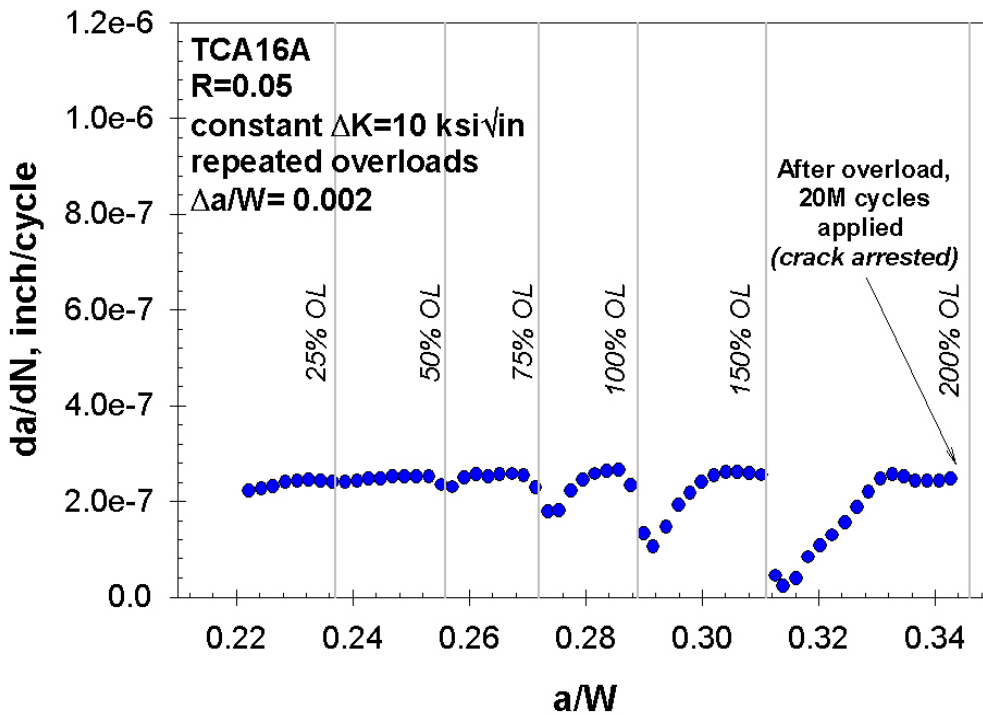


Figure 13. Growth Rate as a Function of Normalized Crack Length

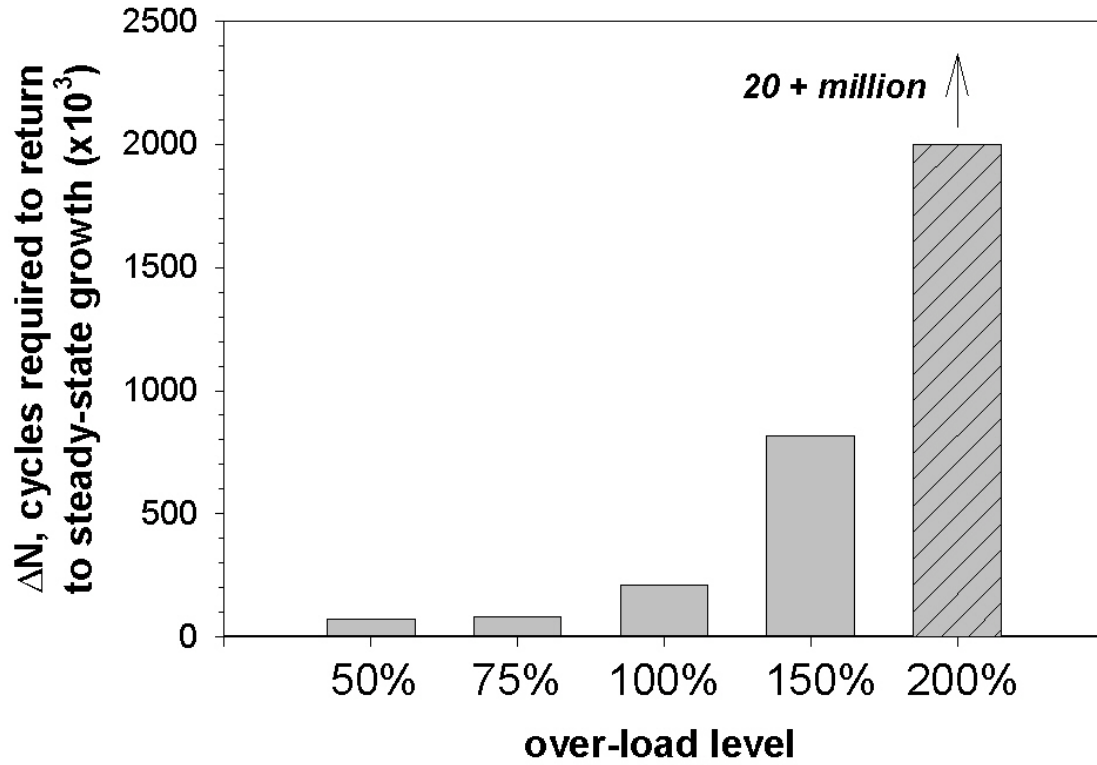


Figure 14. Number of Cycles Needed for Return to Steady-State Crack Growth

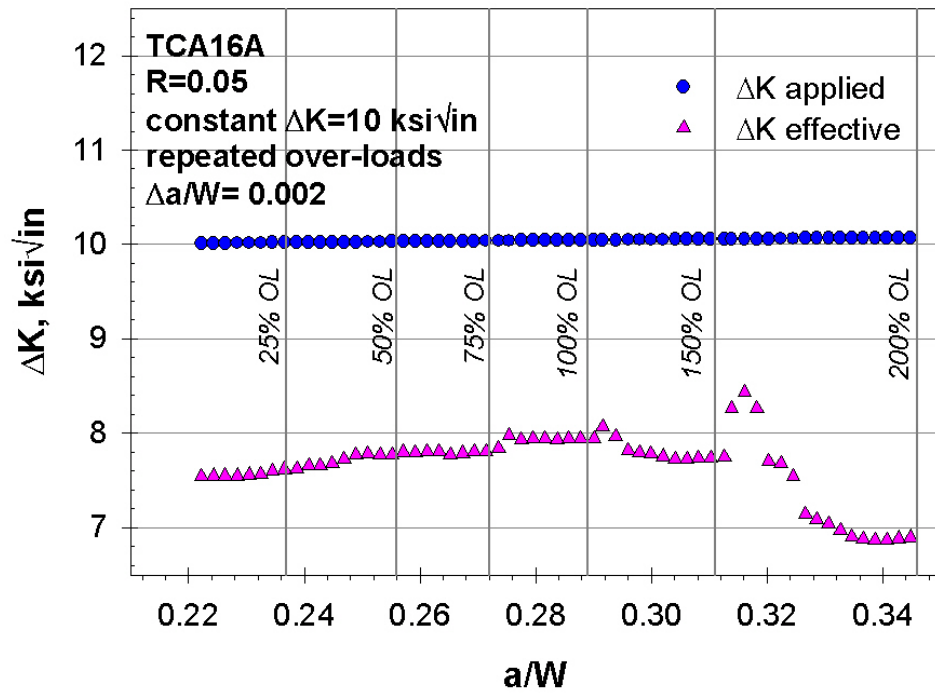


Figure 15. Stress Intensity Range as a Function of Normalized Crack Length

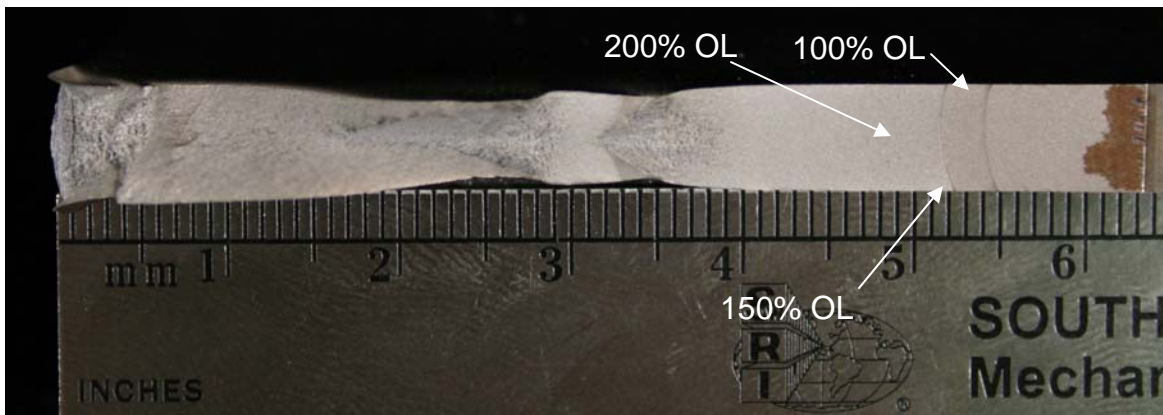


Figure 16. Fracture Surface Showing the Over-Load Events Applied During Testing of TCA16A

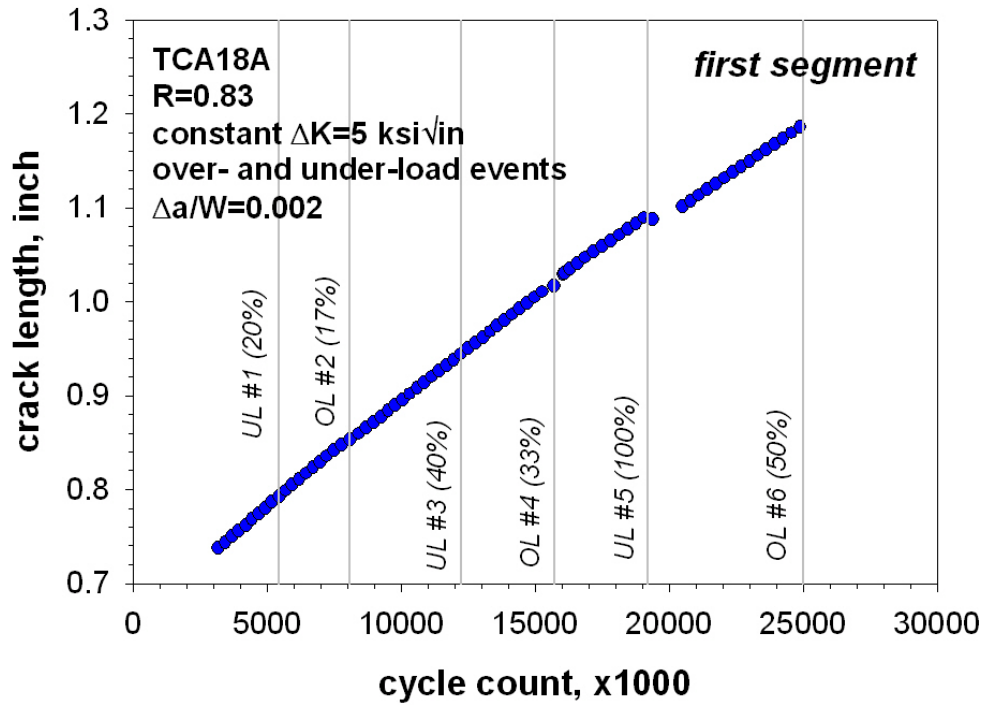


Figure 17. Crack Length versus Cycle Count for TCA18A (First Segment)

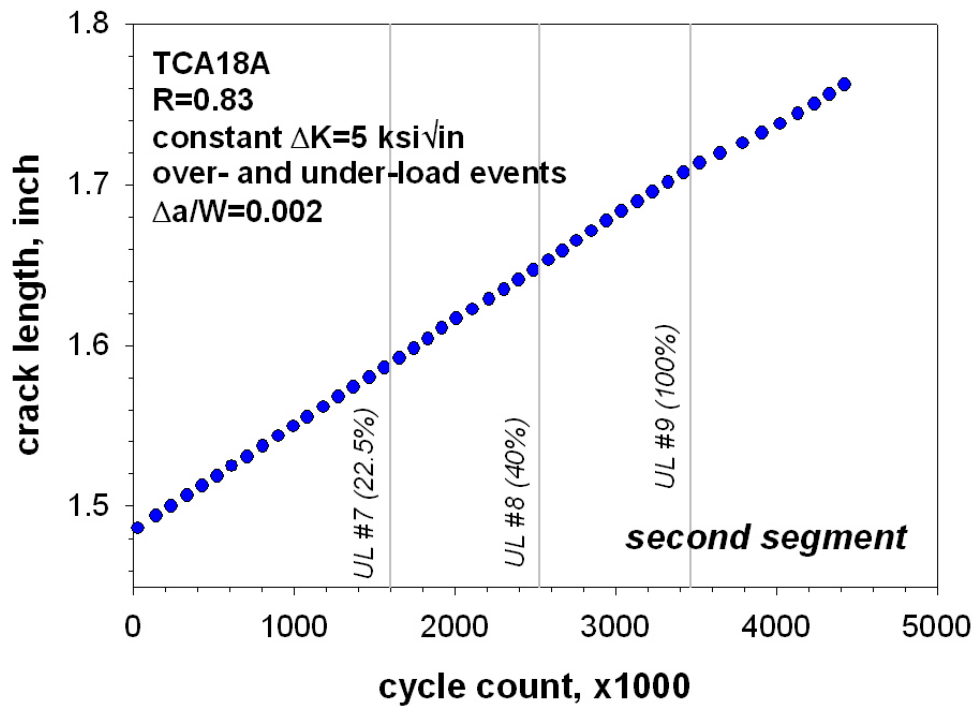


Figure 18. Crack Length versus Cycle Count for TCA18A (Second Segment)

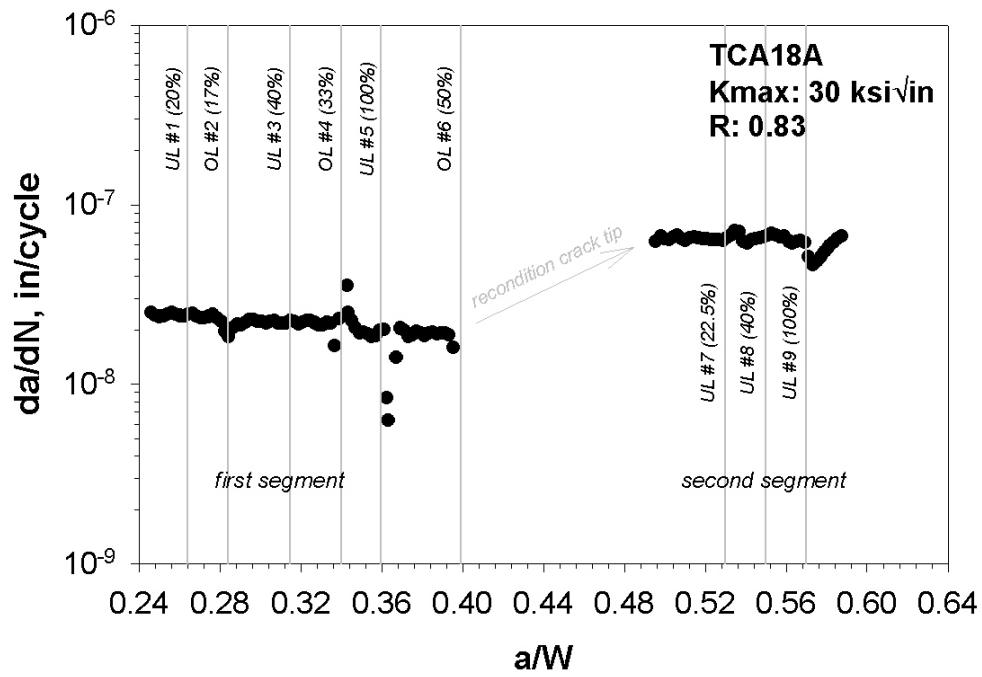


Figure 19. Crack Growth Rate as a Function of Normalized Crack Length (Events Shown)

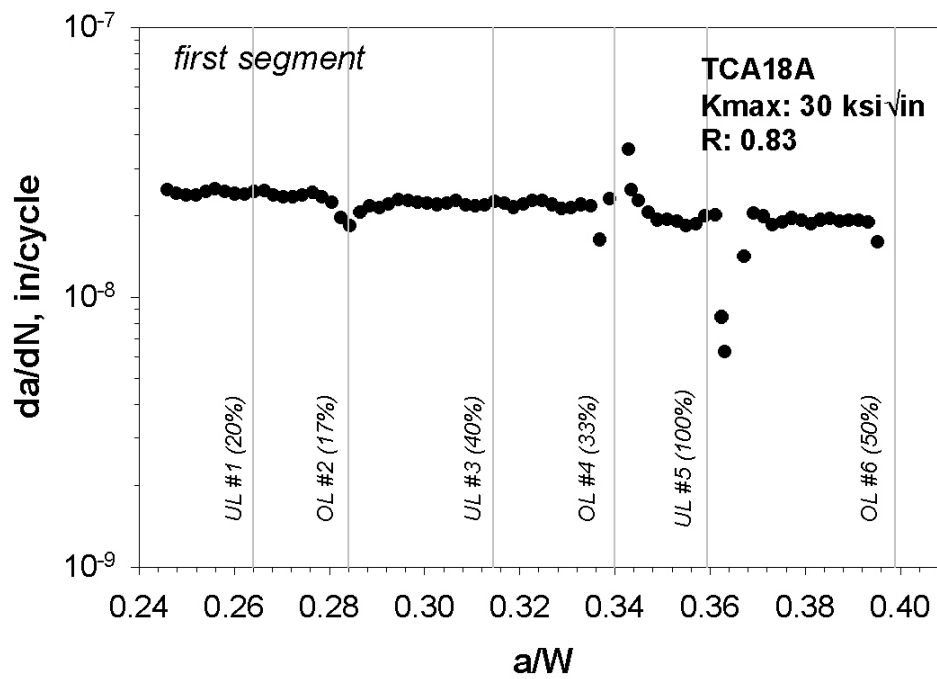


Figure 20. Crack Growth Rate versus Normalized Crack Length (First Segment)

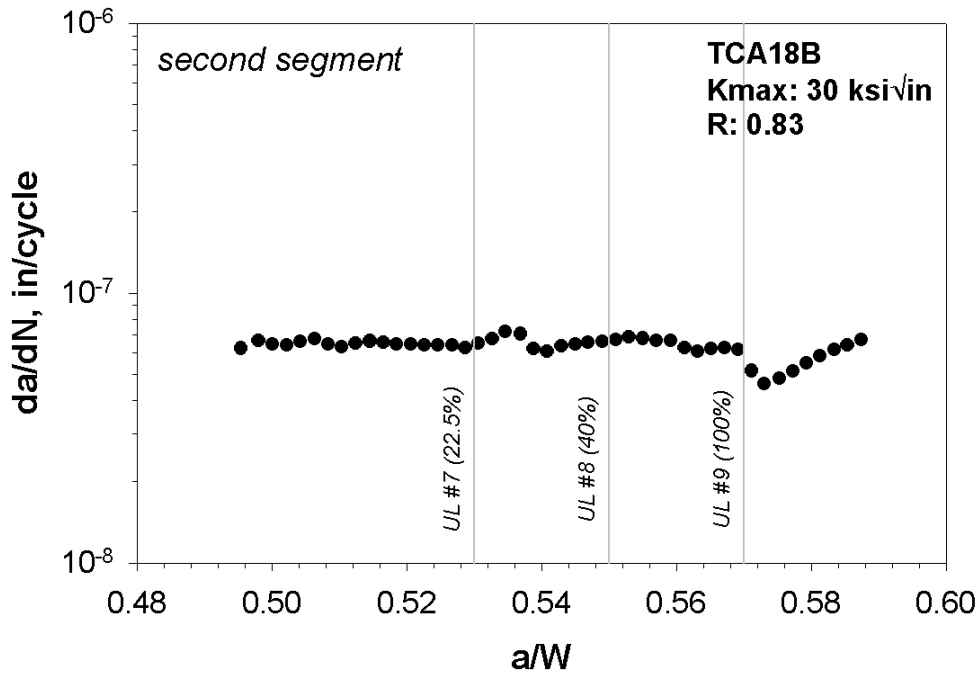


Figure 21. Crack Growth Rate versus Normalized Crack Length (Second Segment)

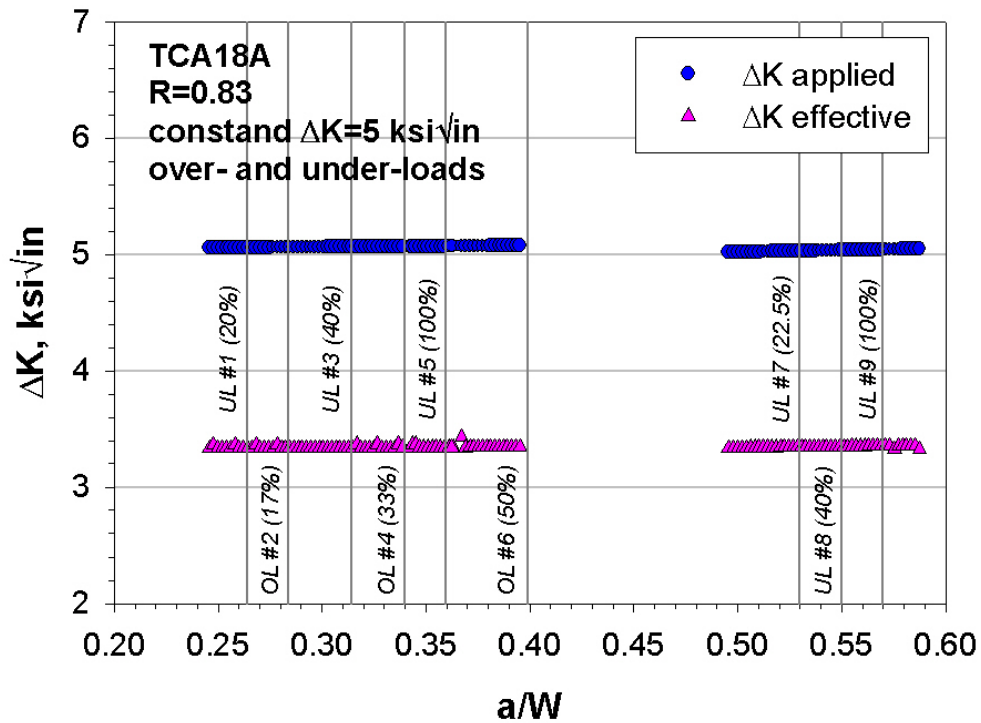


Figure 22. Stress Intensity Range as a Function of Normalized Crack Length

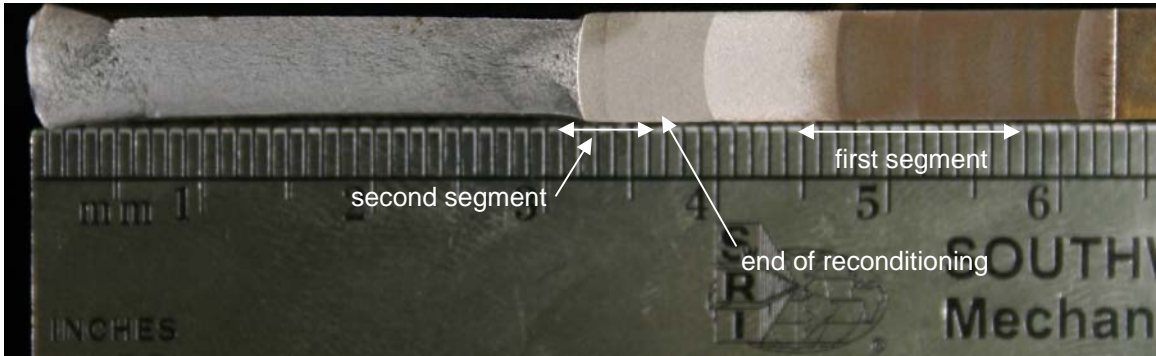


Figure 23. Fracture Surface Showing the Over-Load Events Applied During Testing of TCA18A

5. Conclusions

1. The fully reversed ($R = -1$) FCG data gathered in this program replicated the previous fully reversed data. A slight deviation in the FCG rate was experienced at the higher ΔK levels, although it is within the typical scatter of growth data.
2. Crack closure levels on the order of 40-50 percent were observed in the $R = -1$ test over the range of ΔK analyzed. Closure levels were analyzed at 2 and 5 percent. The trends demonstrated in the reduced displacement plot(s) were typical of crack closure data.
3. Over-load effects at $\Delta K = 10 \text{ ksi}\sqrt{\text{in}}$, $R = 0.05$, manifested at over-loads greater than 50 percent. Significant levels of transient growth rate behavior (retardation) were evident at 75 percent over-load and higher. This type of behavior is common and well documented in engineering alloys. The over-load events starting at 100 percent can be seen on the fracture surface.
4. At 200 percent over-load, crack growth arrest occurred. Cycling continued for 20+ million cycles with no indication of crack growth.
5. Crack closure decreased slightly as over-load level increased to 100 percent. Over-load levels exceeding 100 percent, however, demonstrated a slight decrease in crack closure followed by an increase in crack closure.
6. For the $\Delta K = 5 \text{ ksi}\sqrt{\text{in}}$, $R = 0.833$ load interaction test, fewer load interaction effects were noted. The transient growth behavior after an over-load/under-load was minimal. However, at the 50 percent over-load, crack arrest did occur. The application of under-loads caused slight transient behavior, but steady-state crack growth quickly returned to steady-state levels.

Appendix A

Example of Crack Closure Analysis (Creation of the Reduced Displacement Data)

* * * CLOSURE LOAD ANALYZER * * *

INPUT VALUES:

Input file = tcb6a15a.dat
 Consists of = 20 junklines and 2 chans
 Key Chans = No. 1 (load 3.5 kip/volt)
 No. 2 (disp, polarity = 1.0)
 Anal start/stop = 1683,2802 (cycle No. 2)
 Big Intervals = 10 or 10.000%
 Small Intervals = 2 or 5.000%

LOAD TRIGGERS (kip):

Max Load = 12.208 (90%) Max Unload = 12.208 (90%)
 Min Load = 8.817 (65%) Min Unload = 8.817 (65%)

DATASET EXTREMES (kip, volt):

Max Load = 13.565 Max Strain = 1.858
 Min Load = 0.029 Min Strain = 0.120

DATASET COMPLIANCE:

Unloading-C = 0.138 Int = -0.015 Var = 0.0009 for 141 pts
 Loading-C = 0.140 Int = -0.047 Var = 0.0007 for 141 pts

SEGMENTAL ANALYSIS:

Seg	Unload Segments					Loading Segments				
	#PTS	Pmin	Pmean	Var	CompOff	#PTS	Pmin	Pmean	Var	CompOff
1	57	*****	*****	0.0008	0.92	57	*****	*****	0.0008	-0.88
2	58	*****	*****	0.0009	0.28	58	*****	*****	0.0007	-0.74
3	57	*****	*****	0.0008	-0.07	58	*****	*****	0.0006	-0.14
4	56	*****	*****	0.0007	-0.66	56	*****	*****	0.0008	0.23
5	57	9.513	*****	0.0007	0.23	56	9.489	*****	0.0008	0.24
6	57	8.844	9.527	0.0007	0.80	57	8.811	9.492	0.0006	-0.44
7	57	8.156	8.825	0.0007	0.24	57	8.119	8.813	0.0006	0.17
8	57	7.489	8.172	0.0007	-0.37	57	7.457	8.135	0.0007	1.15
9	57	6.801	7.469	0.0007	-0.41	56	6.790	7.469	0.0007	1.81
10	57	6.138	6.815	0.0007	-0.30	56	6.114	6.792	0.0006	0.61
11	56	5.452	6.125	0.0008	-0.66	58	5.434	6.114	0.0005	0.89
12	57	4.790	5.459	0.0008	-1.10	58	4.755	5.436	0.0008	1.49
13	57	4.097	4.781	0.0010	-0.54	57	4.075	4.748	0.0011	2.98
14	57	3.421	4.103	0.0015	6.71	57	3.382	4.069	0.0014	9.61
15	57	2.750	3.426	0.0008	11.73	56	2.733	3.404	0.0008	14.81
16	57	2.066	2.750	0.0008	13.08	56	2.056	2.725	0.0008	16.45
17	57	1.386	2.071	0.0008	14.71	58	1.356	2.047	0.0009	17.73
18	57	0.709	1.391	0.0034	27.61	57	0.700	1.382	0.0041	30.87
19	57	0.029	0.712	0.0015	44.66	57	0.029	0.681	0.0010	48.93

SEGMENTAL SUMMARY (compl. off.):

Linear	Unload	Loading
Min:	-0.66	-0.88
Mean(-):	-0.36 (2)	-0.59 (3)
Mean(+):	0.56 (4)	0.23 (2)
Max:	0.92	0.24

Global

Max: 44.66 48.93

CLOSURE LOADS:

Absolute Criteria	Loads (kip)		Load Ratio		Status	
	Unload	Load	Unload	Load	Unload	Load
1%:	4.637	5.991	0.342	0.442	ok	ok
2%:	4.543	5.200	0.335	0.383	ok	ok
5%:	4.263	4.541	0.314	0.335	ok	ok
Biased Criteria						
Mean(+)+1%:	4.585	5.728	0.338	0.422	ok	ok
Mean(+)+2%:	4.491	5.093	0.331	0.375	ok	ok
Mean(+)+5%:	4.211	4.517	0.310	0.333	ok	ok
Max(+)+1%:	4.551	5.720	0.335	0.422	ok	ok
Max(+)+2%:	4.457	5.090	0.329	0.375	ok	ok
Max(+)+5%:	4.177	4.517	0.308	0.333	ok	ok

Acronyms and Abbreviations

ASTM	American Society for Testing Materials
C(T)	compact tension
DCPD	direct current potential drop
EDM	electrical discharge machined
FCG	Fatigue Crack Growth
FRA	Federal Railroad Administration
FTA	Fatigue Technology Associates
M(T)	middle-crack tension
NTSB	National Transportation Safety Board
SwRI	Southwest Research Institute
Volpe Center	Volpe National Transportation Systems Center

